

**Manuscript**

**A general route to flame aerosol synthesis and *in situ* functionalization of mesoporous silica**

*Shuo Liu<sup>a</sup>, Chaochao Dun<sup>b</sup>, Junjie Chen<sup>a</sup>, Satyarit Rao<sup>a</sup>, Mihir Shah<sup>a</sup>, Jilun Wei<sup>a</sup>, Kaiwen Chen<sup>a</sup>, Zhengxi Xuan<sup>a,c</sup>, Eleni A. Kyriakidou<sup>a</sup>, Jeffrey J. Urban<sup>b</sup>, and Mark T. Swihart<sup>\*a,c</sup>*

<sup>a</sup>Department of Chemical and Biological Engineering, University at Buffalo, The State University of New York, Buffalo, NY 14260, USA

<sup>b</sup>The Molecular Foundry, Lawrence Berkeley National Laboratory, Berkeley, CA 94720, USA

<sup>c</sup>RENEW Institute, University at Buffalo, The State University of New York, Buffalo, NY 14260, USA

## Abstract

Mesoporous silica is a versatile material for use in catalysis and adsorption in energy, environmental, and medical applications. Here, for the first time, we report a flame aerosol synthesis method for a class of mesoporous silica materials with hollow, amorphous structure, low density, and specific surface area exceeding 1000 m<sup>2</sup>/g. We show its superior performance vs. MCM-41 in properties relevant to water purification, drug carrier, and thermal insulation applications. Moreover, we produced several types of mesoporous silica-supported nano-catalysts by *in situ* incorporation of active metals. The generality of this method is demonstrated by decorating mesoporous supports with noble metal, transition metal, and metal oxide nanoclusters, including Pt/SiO<sub>2</sub>, Ni/SiO<sub>2</sub>, CrO<sub>3</sub>/SiO<sub>2</sub>, and Co/Al<sub>2</sub>O<sub>3</sub>. As a prototypical application, we demonstrate dry reforming of methane using Ni/SiO<sub>2</sub>, achieving constant 97% CH<sub>4</sub> and CO<sub>2</sub> conversions for more than 200 hours, dramatically outperforming a corresponding MCM-41 supported Ni catalyst. Thus, this work provides a continuous and scalable strategy to produce mesoporous silica nanoshells, and the proposed *in situ* functionalization mechanism may pave the way to flexible catalysts for a diverse range of reactions.

**Keywords:** Flame aerosol process; mesoporous silica; hollow nanoshell; *in situ* functionalization; catalyst; methane reforming

## Introduction

The past 30 years have witnessed a plethora of applications of mesoporous silica materials in catalysis,<sup>1-3</sup> biomedicine,<sup>4-6</sup> CO<sub>2</sub> utilization,<sup>7-9</sup> and electrochemistry.<sup>10-12</sup> For example, mesoporous silica is widely used in heterogeneous catalysis and adsorption because its high porosity facilitates adsorption, and the relatively large pores allow rapid mass transfer, compared to zeolites and other high surface area materials.<sup>1</sup> High specific surface area provides high adsorption capacity or a large number of active sites per mass.<sup>13,14</sup> To date, the vast majority of mesoporous silica materials have been synthesized in the liquid phase, which enables bottom-up construction of complex hierarchical structures. However, this approach often encounters barriers to commercial implementation due to time-consuming batch processing and undesirable variations of physicochemical properties upon scale-up.<sup>15-17</sup>

Flame aerosol processing, the most common method for industrial

production of low-cost nanomaterials (e.g. carbon black and fumed silica), has attracted broad interest for preparing advanced nanomaterials over the past twenty years.<sup>18-20</sup> However, the synthesis of high porosity mesoporous silica has not been achieved by this scalable method.<sup>18,21</sup> A key challenge is that the high temperature of conventional flame synthesis (often above 2000 °C) destroys organic surfactants used to template pores in mesoporous materials. Instead, flame synthesis generally produces non-porous nanometer sized silica particles<sup>22-25</sup> (fumed silica) by a gas-to-particle route.<sup>18,21</sup> While such fumed silica particles can have high surface area (typically up to 500 m<sup>2</sup>/g),<sup>22</sup> they do not have internal mesopores, but take the form of fractal aggregates. Over the past several years, our group has developed a novel flame-based aerosol reactor in which particle formation takes place at lower temperature.<sup>26-28</sup> Specifically, our reactor separates the flame and particle formation processes into different regions, instead of producing particles in the flame as in traditional flame spray pyrolysis. With an aqueous precursor solution, this yields much lower particle formation temperatures that favor a droplet-to-particle route rather than a gas-to-particle route to particle formation, particularly for silica and other oxides. Such a mechanism provides opportunities to achieve surfactant self-assembly and inorganic macromolecule sol-gel growth processes within each droplet, finally producing mesopores after the removal of the template from the silica

matrix. Interestingly, the hollow nanoshell structure is intrinsically formed without introducing a second template. The flame synthesized mesoporous silica nanoshell provides properties with advantages over conventional MCM-41 in water purification, insulation, and drug delivery fields.

Here, we demonstrate both flame-driven aerosol-assisted self-assembly to produce mesoporous hollow silica spheres, and *in situ* formation of highly dispersed catalytically active sites on the mesoporous silica by addition of metal salts into the silica precursor solution. On one hand, we synthesized mesoporous silica nanoshells with BET specific surface area exceeding 1000 m<sup>2</sup>/g and extended this method to other porous ceramic materials. On the other hand, we successfully incorporated multiple types of nanoclusters within the mesoporous silica, including noble metal (Pt/SiO<sub>2</sub>), transition metal (Ni/SiO<sub>2</sub>), and metal oxide (CrO<sub>3</sub>/SiO<sub>2</sub>) active sites, and also explored porous alumina as a support material (Co/Al<sub>2</sub>O<sub>3</sub>). Broad applications of these supported nanoparticles can be envisioned. As a typical example, the flame synthesized Ni/SiO<sub>2</sub> was tested as a catalyst for the dry reforming of methane ( $\text{CH}_4 + \text{CO}_2 \leftrightarrow 2\text{H}_2 + 2\text{CO}$ ), for which it exhibited exceptional activity and stability at high reaction temperature, significantly out-performing a conventional catalyst synthesized by wet-impregnation of Ni nanoparticles onto an MCM-41 mesoporous silica support.

## Results and discussion

The mesoporous silica nanoshells were produced in a continuous flame aerosol process based on an unconventional flame reactor configuration (**Figure S1, S2**). During the synthesis process, the H<sub>2</sub>-rich flame generates the high temperature in the reaction chamber that drives evaporation and reaction. The injected liquid precursor was instantly atomized into microdroplets and underwent rapid (<0.05 s) self-assembly and a silica nucleation and growth processes, followed by N<sub>2</sub> quenching. Finally, the products were collected on a filter membrane.

A schematic of the mesoporous silica nanoshell formation process is provided in **Figure 1**, which shows evaporation-driven organic template self-assembly and inorganic macromolecule growth by a rapid sol-gel process. Specifically, the initial mesoporous silica precursor droplets consisted of an isotropic mixture of TEOS, CTAB, H<sub>2</sub>O, ethanol, and HCl. Fast solvent evaporation increased the CTAB concentration above its critical micelle concentration, driving CTAB self-assembly into cylindrical micelles. Meanwhile TEOS polycondensation occurred through sol-gel chemistry to precipitate organosilica material on the micelles, finally forming the mesophase particles of hybrid inorganic-organic network. Upon removal of the micelle template and other organic components from

the intermediate product by calcination, mesopores were formed, as evidenced by the dramatic increase of Brunauer-Emmett-Teller (BET) specific surface area from 10 to 1030 m<sup>2</sup>/g after calcination, which is much higher than flame synthesized silica powder produced without CTAB in the precursor solution (**Table S1**).

A hollow nanoshell structure is intrinsically formed because solvent evaporation occurs at the outer surface of each droplet, producing the highest precursor and surfactant concentration at the surface, such that silica formation starts from the surface. Because the diffusivity of the solutes (precursor, surfactant, and growing silica clusters) is much lower than that of the evaporating solvent, the mesoporous silica grew inward from the surface as water diffused out, finally yielding a hollow particle. Such a droplet to hollow particle conversion requires rapid heating to drive evaporation on a time scale too short for precursor diffusion to make the concentrations within the droplet uniform. At slower heating rate, solid silica particles<sup>29-31</sup> or micron-sized silica spheres with large hollow voids and thick shells<sup>32-34</sup> will be produced, as in relative mild spray-drying-based aerosol synthesis processes.

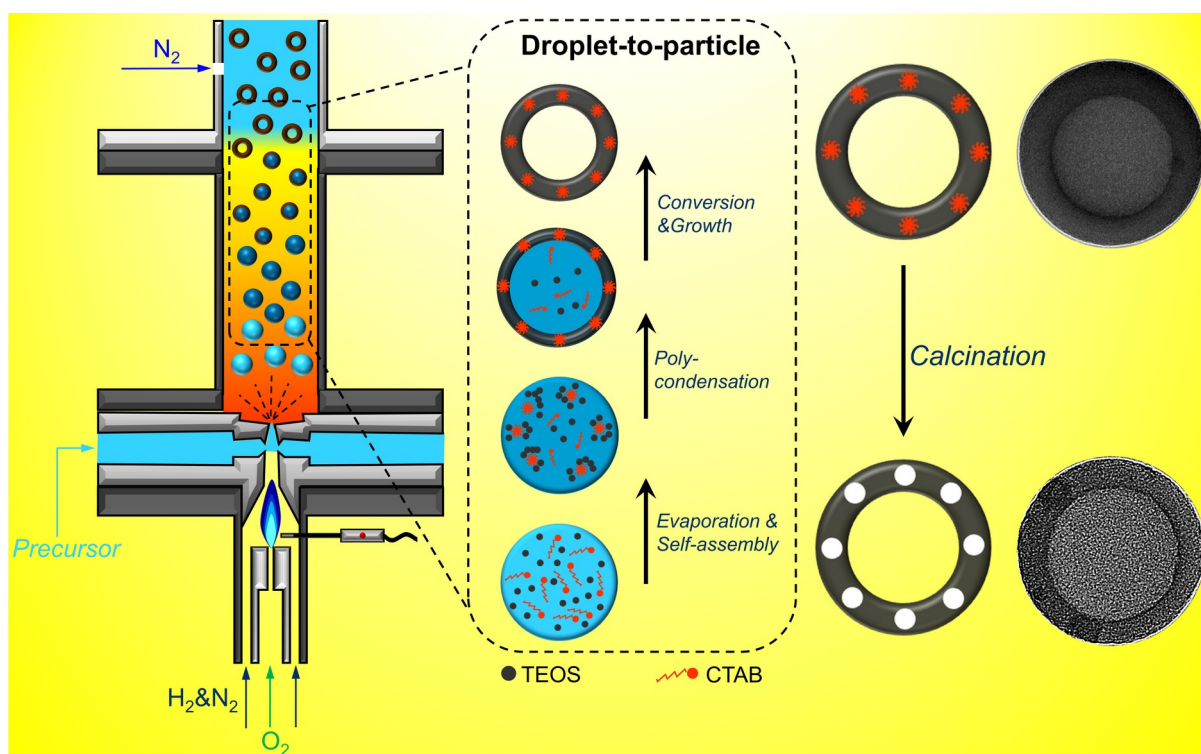


**Figure 1.** Schematic of mesoporous silica nanoshell formation process.

Adjusting reaction parameters (precursor concentrations, temperature, pressure, surfactant concentration, etc.) in the flame aerosol process allows flexible tailoring of the mesoporous silica to achieve desired characteristics.<sup>18,20,21</sup> **Tables S2-S4** summarize the optimization of BET surface area, pore volume and porosity (or average pore width) with regard to catalytic applications of interest, where competitive values of 1030 m<sup>2</sup>/g, 0.850 cm<sup>3</sup>/g, and 3.12 nm were achieved, respectively. Beyond that, **Table S5** presents the variation of density as a function of the CTAB/TEOS molar ratio. The tap density decreases to 0.015 g/cm<sup>3</sup> for a CTAB/TEOS molar ratio of 0.08. Moreover, adopting lower TEOS concentration (30 mM) and higher reaction chamber temperature (850 °C)

produced almost exclusively hollow nanospheres with a geometric mean diameter of 230 nm (**Figure S3**). Although the BET surface area and pore volume were lower than the sample in **Figure 2**, the large void space and thin shell of this sample might provide better performance in some particular applications, such as CO<sub>2</sub> capture<sup>35</sup>.

For the optimized material, transmission electron microscopy (TEM) images revealed that most particles exhibit a hollow nanoshell morphology with dense and disordered mesoporous structure (**Figure 2a**). The corresponding selected area electron diffraction (SAED) and powder X-ray diffraction (XRD) analysis showed the amorphous structure of the flame synthesized mesoporous silica. After calcination, Fourier transform infrared spectroscopy (FTIR, **Figure 2b**) showed SiO<sub>2</sub> with isolated silanol groups indicated by the peak at 1620 cm<sup>-1</sup>.<sup>36,37</sup> Thermogravimetric analysis and differential scanning calorimetry (TGA-DSC, **Figure S4c**) demonstrated that most of the micelle template was removed between 200 and 400 °C. N<sub>2</sub> sorption measurements like those in **Figure 2c** showed type IV isotherms, consistent with the material's mesoporous structure.<sup>38</sup> The adsorption/desorption isotherms presented a H2 type of hysteresis loop in the P/P<sub>0</sub> range of 0.40~0.95, reflecting delayed N<sub>2</sub> evaporation from hollow voids that are blocked by the mesoporous wall.<sup>39</sup> The Barrett-Joyner-Halenda (BJH) pore size distribution

showed the pores of 1~5 nm in the wall (**Figure 2d**), while the small peak above 100 nm is likely due to the hollow voids.

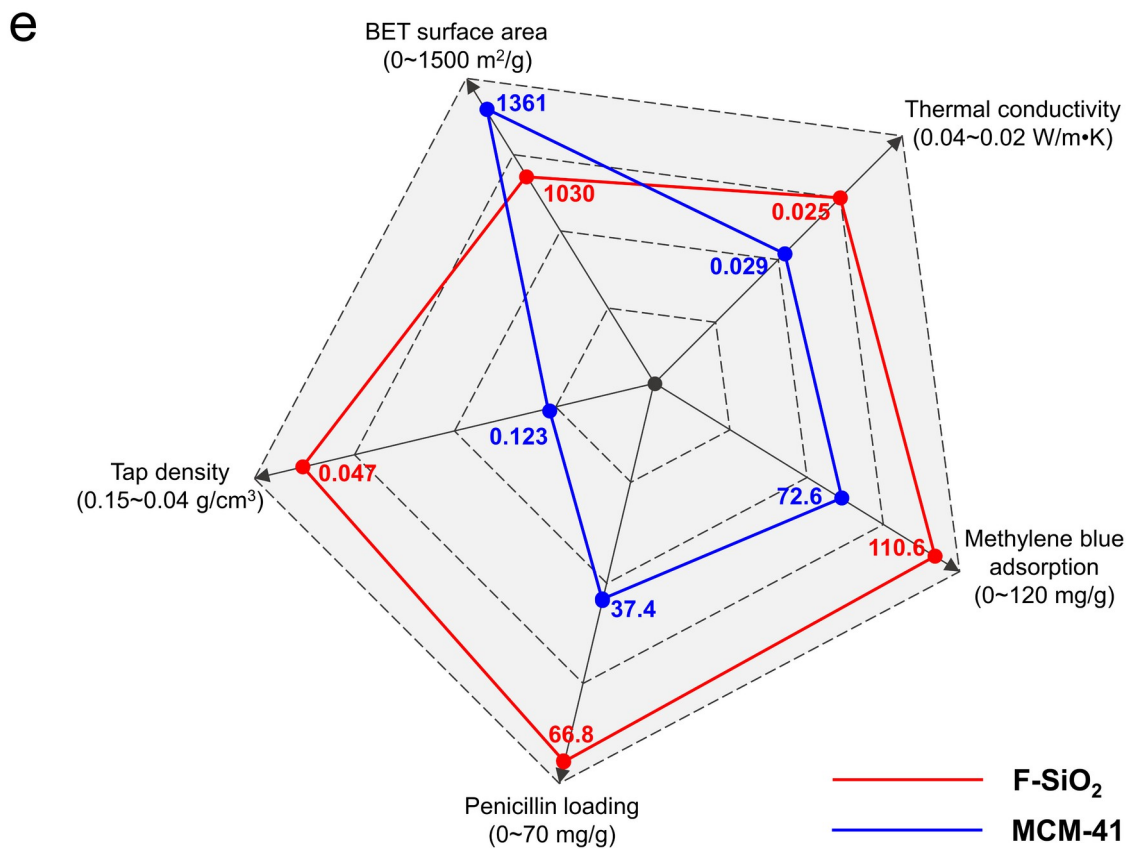
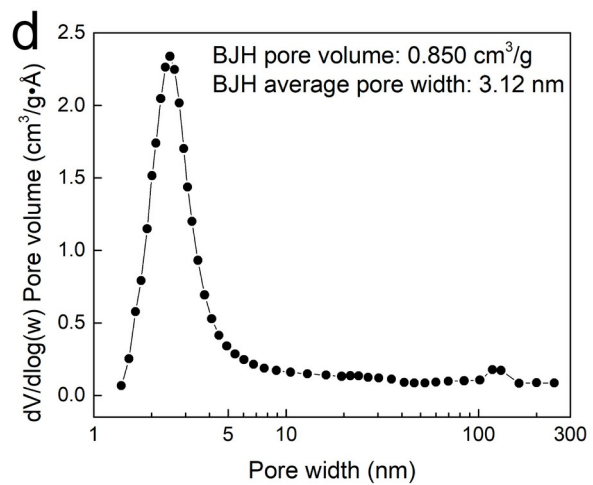
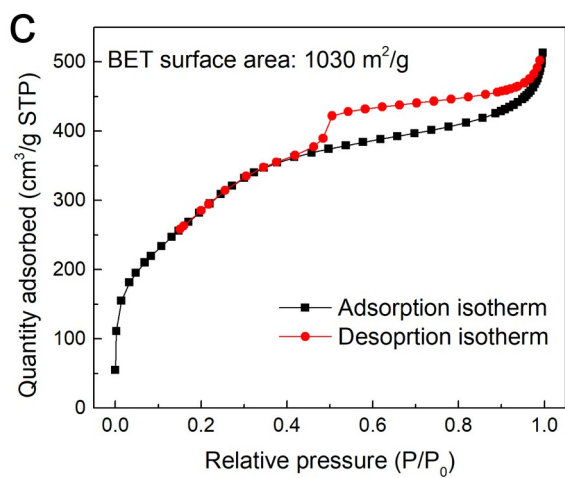
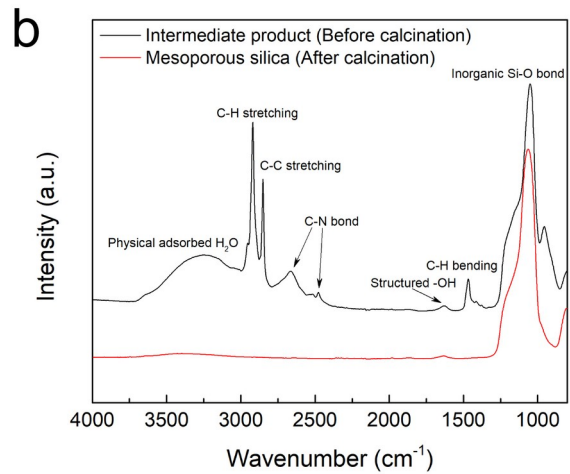
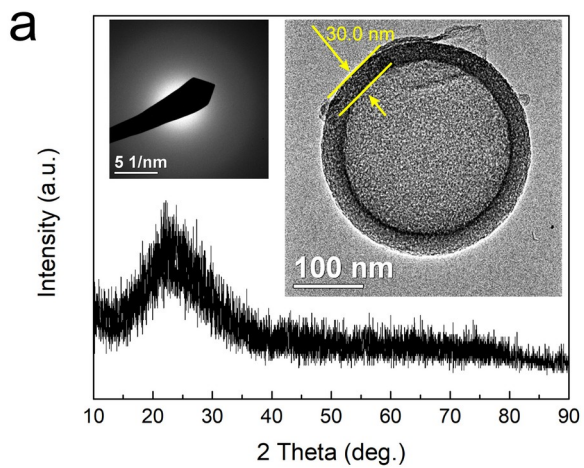


**Figure 2.** Characterizations and applications of flame synthesized mesoporous silica (F-SiO<sub>2</sub>). **a.** XRD pattern, TEM image and SAED pattern; **b.** FTIR spectra of intermediate and final products; **c.** N<sub>2</sub> adsorption/desorption isotherms and **d.** BJH adsorption pore width distribution curve. This representative sample is the second one highlighted in **Table S4**, and other supplementary characterization of this sample is shown in **Figure S4**. **e.** Comprehensive comparisons between F-SiO<sub>2</sub> and MCM-41 with respect to BET surface area, tap density, and properties relevant to applications in water purification (methylene blue dye adsorption), drug delivery (penicillin loading) and thermal insulation (thermal conductivity) applications.

The high surface area and hollow void of the flame synthesized mesoporous silica (F-SiO<sub>2</sub>) provide high capacity for molecular adsorption and loading, which are desirable properties in water purification<sup>40</sup> and drug delivery<sup>41</sup> applications. Meanwhile, the ultra-low density (**Table S5**) of F-SiO<sub>2</sub> is even comparable to ultralight aerogels that have great potential as thermal insulation materials.<sup>42,43</sup> To further confirm these possibilities, we performed representative methylene blue dye adsorption, penicillin loading and thermal conductivity tests of the F-SiO<sub>2</sub> sample shown in **Figure 2**, and made comprehensive comparisons with the prototypical mesoporous silica material, MCM-41. Both F-SiO<sub>2</sub> and MCM-41 were directly used in these tests without any post-treatment or surface modification operations. In general, the MCM-41 exhibited ordered hexagonal pores, uniform particle size, and a higher BET surface area (1361 m<sup>2</sup>/g) than F-SiO<sub>2</sub> (**Figure S5**). However, as shown in **Figure 2e**,

the F-SiO<sub>2</sub> presented a higher capacity for dye adsorption and drug loading, as well as ultra-low density and thermal conductivity, and showed overall advantages over MCM-41 in these respects. These results suggest that the porous, hollow, ultralight, and low-cost F-SiO<sub>2</sub> material could have great potential in numerous energy, environmental, and medical applications.

We further extended this method to other porous ceramic materials, like Al<sub>2</sub>O<sub>3</sub>. TEM images clearly showed a porous structure (**Figure S6b**). Because of the weaker interaction between the inorganic Al precursor and micelle template, the BET surface area (120 m<sup>2</sup>/g) of mesoporous Al<sub>2</sub>O<sub>3</sub> was not nearly as high as for mesoporous silica. Nevertheless, the specific surface area was dramatically higher than that of Al<sub>2</sub>O<sub>3</sub> nanoshells synthesized without CTAB in the precursor.<sup>44</sup>

Hollow-structured mesoporous materials combine a large interior void space with mesoporous channels in the shell, providing high permeability for mass transfer of reactants as catalyst supports.<sup>45</sup> We further demonstrated an *in situ* functionalization strategy by decorating silica with noble metal, transition metal, and metal oxide active nanoclusters and also using porous alumina as a catalyst support. We further characterized one typical sample for each combination, including 1 wt.%

Pt/SiO<sub>2</sub>, 5 wt.% Ni/SiO<sub>2</sub>, 5 wt.% CrO<sub>3</sub>/SiO<sub>2</sub>, and 5 wt.% Co/Al<sub>2</sub>O<sub>3</sub>. More fabrication details are given in the Supporting Information. As expected, the porosity decreased after loading nonporous, higher-density active materials (**Table S6**). High-angle annular dark-field scanning transmission electron microscopy (HAADF-STEM) and elemental mapping images confirmed good dispersion, high loading level, and limited aggregation of active sites for each of these catalysts (**Figure 3b-e**).

The *in situ* functionalization mechanism for systematic decoration of active sites within the mesoporous silica is shown in **Figure 3a**. The particle formation mechanisms in flame aerosol synthesis depends on multiple factors such as precursor composition and concentration, temperature, pressure, and reactor configuration.<sup>18,20,21</sup> In this study, the catalyst precursor was a mixture of metal nitrate salt and silica (or alumina) precursor. The silica support followed the same droplet-to-particle conversion shown in **Figure 1**, and finally formed the mesoporous nanoshell structure. For the active sites, both gas-to-particle and droplet-to-particle conversion processes are possible: In a gas-to-particle route, the metal precursor was first pyrolyzed into product vapor. Afterwards, some active nanoparticles were produced by homogeneous nucleation in the gas phase and deposited onto the silica surface. At the same time, some vapor directly deposited on the silica (heterogeneous nucleation)

such that nanoparticles grew on the silica surface. Therefore, the gas-to-particle mechanism often produces larger nanoclusters on the silica surface. In contrast, in the droplet-to-particle route, active sites formed together with silica in the droplet phase, which produces nanoclusters embedded within the silica.

Specifically, 1 wt.% Pt/SiO<sub>2</sub> followed a droplet-to-particle conversion, which produced highly dispersed Pt nanoclusters within the silica (**Figure 3b**, **Figure S7a, b**). The high dispersion and narrow particle size distribution of Pt nanoclusters were maintained after thermal reduction treatment at 700 °C. This is consistent with the XRD analysis, which showed no distinct features of Pt but only a weak peak at a  $2\theta \sim 41^\circ$  (**Figure S7c**). The weak signal of Pt zero-valent state at 75 eV from X-ray photoelectron spectroscopy (XPS, **Figure S7d**) indicated Pt was absent on the surface (depth limitation of XPS is c.a. 5 nm), which further confirmed the droplet-to-particle conversion mechanism. Notably, the dispersion and density of Pt were much higher than the Pt/SiO<sub>2</sub> prepared through spray-drying aerosol technology (Pt >10 nm),<sup>46</sup> benefiting from the rapid and violent material formation process of flame aerosol synthesis. The as-synthesized Pt/SiO<sub>2</sub> has potential as a heterogeneous catalyst for reactions such as CO oxidation,<sup>47</sup> ethylene oxidation,<sup>48</sup> and toluene hydrogenation.<sup>49</sup>

5 wt.% Ni/SiO<sub>2</sub> showed evidence of both gas-to-particle and droplet-to-particle conversion processes. On one hand, a homogeneous distribution of small Ni nanoclusters was evident within the silica nanoshell (**Figure 3c**); On the other hand, Ni nanoparticles with diameter more than 10 nm were also observed on the silica surface (**Figure S8a, b**). The XRD pattern of this sample showed obvious Ni peaks that further demonstrated the presence of relatively larger Ni nanoparticles on the silica surface (**Figure S8c**). The XPS spectra showed both Ni<sup>0</sup> and Ni<sup>2+</sup> because of the slight oxidation of surface atoms of Ni nanoparticles in air (**Figure S8d**). The as-synthesized Ni/SiO<sub>2</sub> has potential applications in catalysis of methane reforming,<sup>50</sup> CO<sub>2</sub> methanation,<sup>51</sup> ammonia decomposition<sup>52</sup> and other reactions.

Finally, 5 wt.% CrO<sub>3</sub>/SiO<sub>2</sub> followed a droplet-to-particle conversion route, demonstrated by the presence of CrO<sub>3</sub> nanoclusters homogeneously distributed within the silica (**Figure 3d**). TEM observations (**Figure 3d, Figure S9a, b**) confirmed the ultra-small particle size and high density of CrO<sub>3</sub> nanoclusters within silica, without any aggregation. XRD showed no CrO<sub>3</sub> peaks (**Figure S9c**) even with a high loading of 5 wt.%, further demonstrating the ultra-small particle size. The chromium attained the maximum valence of Cr<sup>6+</sup> after calcination in air (**Figure S9d**). The as-synthesized CrO<sub>3</sub>/SiO<sub>2</sub> has potential applications in catalytic reactions such

as ethane dehydrogenation,<sup>53</sup> propane dehydrogenation<sup>54</sup> and ethylene polymerization.<sup>55</sup>

Similarly, 5 wt.% Co/Al<sub>2</sub>O<sub>3</sub> also followed a droplet-to-particle route (**Figure 3e**), in which Co nanoparticles were produced by exsolution behavior in a reducing atmosphere. Similar to previous studies,<sup>56,57</sup> a rapid material formation process followed by fast quenching enabled incorporation of immiscible elements into a single phase. In this case, the obtained Co-Al<sub>2</sub>O<sub>3</sub> has an amorphous ceramic solid solution structure (**Figure S10a**), as evidenced by the XRD pattern with no Co peaks before thermal reduction (**Figure S10c**). After reduction, the reducible transition metal can be exsolved from the host lattice,<sup>58,59</sup> to produce metallic Co nanoparticles on the alumina surface (**Figure S10b**), as confirmed by XRD and XPS (**Figure S10c, d**). Previous studies demonstrated that active sites generated by exsolution often provide strong metal-support interactions that limit metal sintering at high reaction temperature.<sup>60,61</sup> Thus, the Co/Al<sub>2</sub>O<sub>3</sub> hollow porous nanospheres have potential applications in Fischer-Tropsch synthesis,<sup>62</sup> propane dehydrogenation<sup>63</sup> and methane reforming.<sup>64</sup>

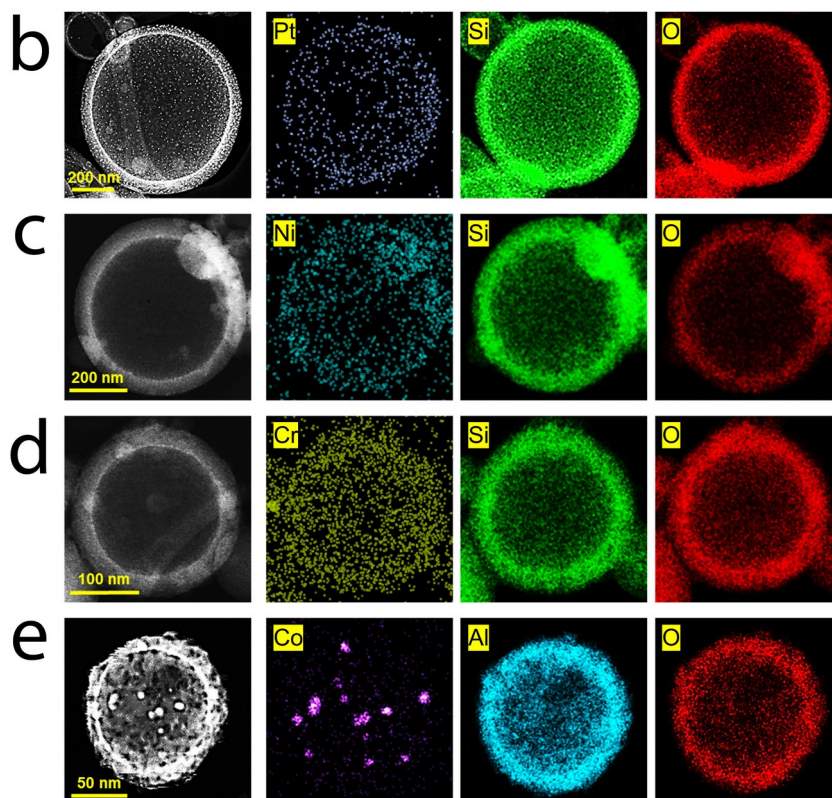
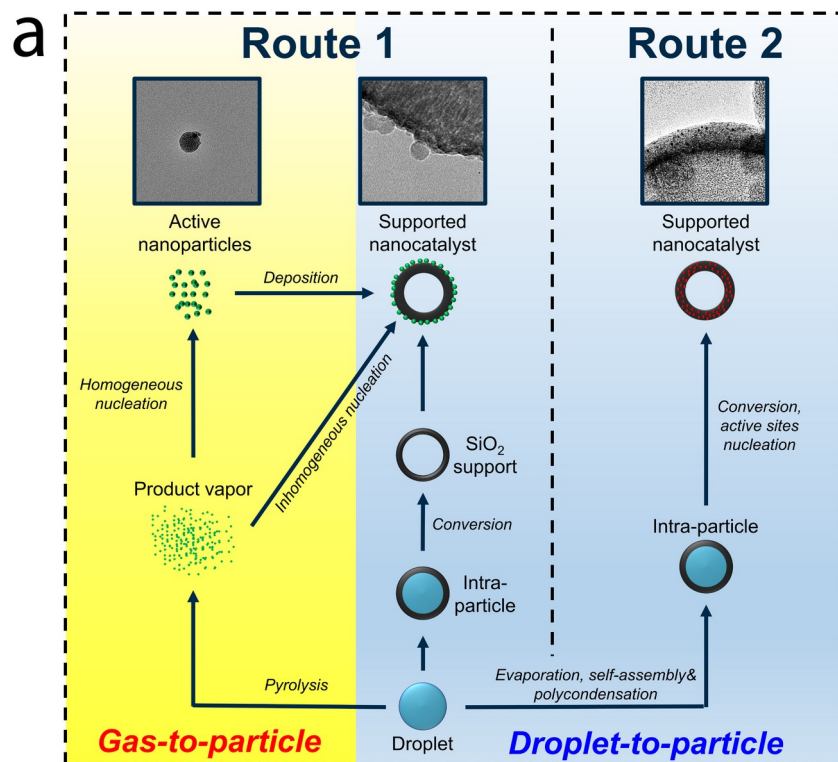


**Figure 3.** *In situ* functionalization of mesoporous nanoshells in a flame aerosol process. **a.** Schematic of decorating active nanoparticles by gas-to-particle and droplet-to-particle conversion processes; HAADF-STEM and elemental mapping images of representative as-synthesized mesoporous nanoshell supported catalysts: **b.** 1 wt.% Pt/SiO<sub>2</sub>, **c.** 5 wt.% Ni/SiO<sub>2</sub>, **d.** 5

wt.% CrO<sub>3</sub>/SiO<sub>2</sub> and **e.** 5 wt.% Co/Al<sub>2</sub>O<sub>3</sub>. More details are provided in supporting information **Figure S7-S10**.

The above *in situ* functionalization method enables the rational design of a large library of mesoporous nanoshell supported nanocatalysts. As a typical example, the flame synthesized Ni/SiO<sub>2</sub> (Ni/F-SiO<sub>2</sub>) was tested as a catalyst for the dry reforming of methane reaction (**Figure 4a**), with Ni contents of 2 wt.%, 5 wt.%, 7 wt.%, 10 wt.%, and 15 wt.% (**Figure S11**). When the Ni content was below 10 wt.%, the Ni/F-SiO<sub>2</sub> showed relatively low and decreasing CH<sub>4</sub> conversion after 50 hours. However, upon increasing Ni content to 15 wt.%, the Ni/F-SiO<sub>2</sub> showed constant 97% CH<sub>4</sub> conversion over 210 hours, which further demonstrated the robustness of mesoporous nano-shells with a large amount of effective active sites. The catalytic activity of Ni/F-SiO<sub>2</sub> was evaluated at varied reaction temperatures as well (**Figure 4b**). CH<sub>4</sub> and CO<sub>2</sub> conversions increased with increasing temperature, as expected for this exothermic reaction. When the reaction temperature was below 800 °C, CH<sub>4</sub> conversion was lower than CO<sub>2</sub> conversion and the H<sub>2</sub>/CO ratio was below 1 due to the reverse water-gas shift (CO<sub>2</sub> + H<sub>2</sub> ↔ CO + H<sub>2</sub>O) side reaction.<sup>65</sup> At 850 °C, the CH<sub>4</sub> and CO<sub>2</sub> conversion were nearly equal, and the H<sub>2</sub>/CO ratio approached 1.

We compared the performance of Ni/F-SiO<sub>2</sub> with a conventional catalyst

prepared by wet-impregnation of Ni on MCM-41 support (Ni/MCM-41). Catalyst stability was assessed by continuous time-on-stream tests at 850 °C (**Figure 4c-e**), where the conversions were the highest. While the Ni/F-SiO<sub>2</sub> retained constant 97% CH<sub>4</sub> and CO<sub>2</sub> conversions for 210 hours, the Ni/MCM-41 showed continuously decreasing catalytic performance, with CH<sub>4</sub> conversion decreasing to 58% and CO<sub>2</sub> conversion decreasing to 80% in 70 hours. These results suggested that the Ni/F-SiO<sub>2</sub> provides dramatically improved activity and stability over Ni/MCM-41, despite the higher BET surface area and ordered hexagonal pore structure of the MCM-41 support (**Figure S5**).

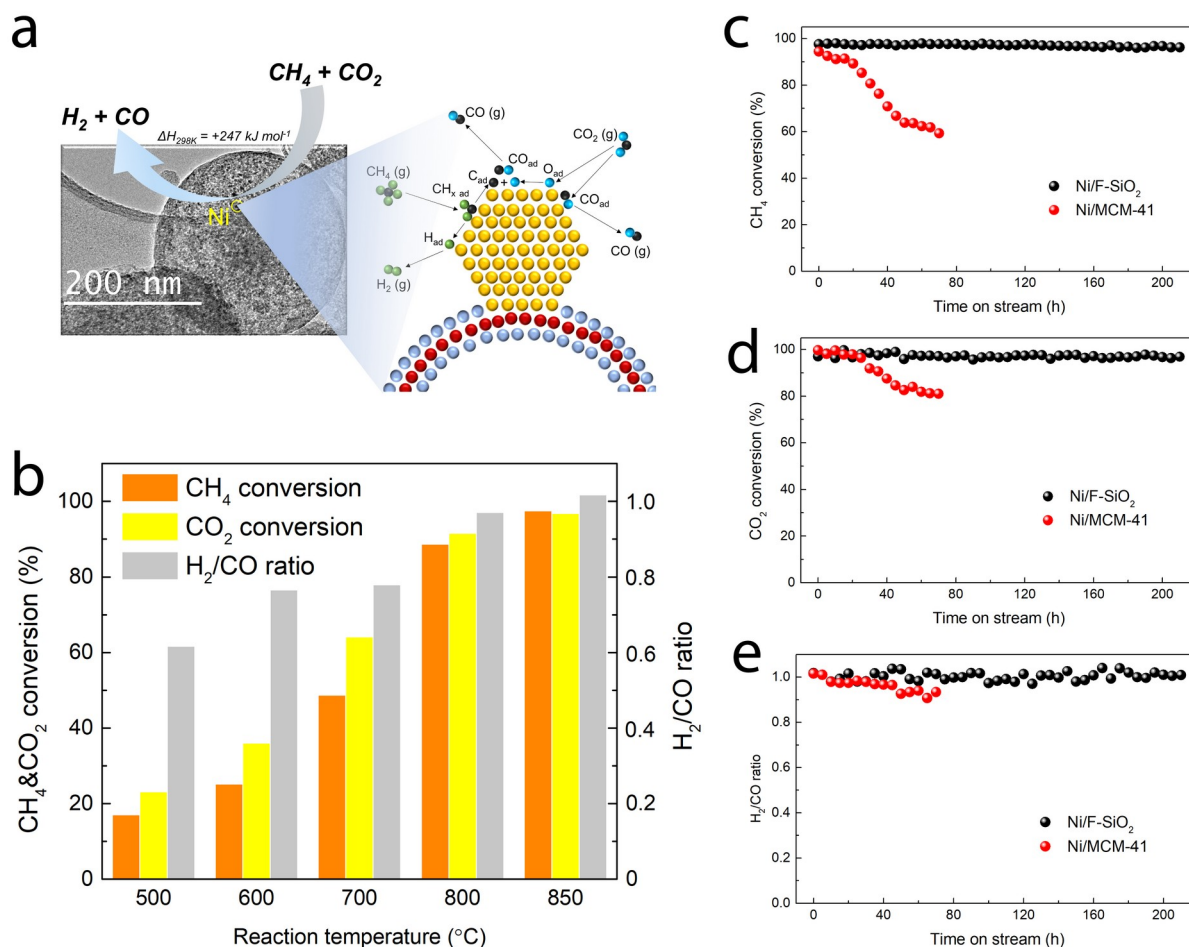


**Figure 4.** A prototypical catalytic application of 15 wt.% Ni/SiO<sub>2</sub> for dry reforming of methane. **a.** Catalytic reaction mechanism of Ni/F-SiO<sub>2</sub>; **b.** CH<sub>4</sub> conversion, CO<sub>2</sub> conversion, and H<sub>2</sub>/CO ratio of Ni/F-SiO<sub>2</sub> catalytic activity test at varied temperatures; **c.** CH<sub>4</sub> conversion, **d.** CO<sub>2</sub> conversion, and **e.** H<sub>2</sub>/CO ratio of Ni/F-SiO<sub>2</sub> and Ni/MCM-41 continuous catalytic stability tests at 850 °C. Reaction conditions: 60 mL/min total stream flow rate, CH<sub>4</sub>:CO<sub>2</sub>:Ar = 1:1:1, 50 mg catalyst loading, 72000 mL g<sub>cat</sub><sup>-1</sup> h<sup>-1</sup> GHSV.

## Conclusions

In summary, we present a new method for synthesis of mesoporous hollow silica and other porous ceramic materials by a flame aerosol process and demonstrate the exceptional properties relevant to water purification, drug carrier and thermal insulation applications that are

achievable by this route. We also propose a generic *in situ* functionalization method to load highly dispersed active nanoparticles onto these mesoporous hollow nanospheres, which opens up a vast compositional space for mesoporous nanoshell supported heterogeneous catalysts discovery. In contrast to traditional wet impregnation that requires many separate steps, the current flame synthesis method incorporates micelle self-assembly, silica sol-gel reactions, and active site loading processes into a single step (**Figure S12**), which produced mesoporous silica supported nanocatalysts in a continuous, scalable, and low-cost route. In a prototypical reaction, the flame-synthesized catalyst exhibited superior activity and stability, further demonstrating the promise of this novel material synthesis route.

## **Acknowledgments**

This work was partially supported by the Molecular Foundry at Lawrence Berkeley National Laboratory by the Office of Science, Office of Basic Energy Sciences of the U.S. Department of Energy (DOE) under Contract No. DE-AC02-05CH11231 and by the U.S. National Science Foundation, grant number CBET-1804996.

## **References**

- 1 Liang, J., Liang, Z., Zou, R. & Zhao, Y. Heterogeneous Catalysis in Zeolites, Mesoporous Silica, and Metal-Organic Frameworks. *Adv. Mater.* **29**, doi:10.1002/adma.201701139 (2017).
- 2 Sun, L. B., Liu, X. Q. & Zhou, H. C. Design and fabrication of mesoporous heterogeneous basic catalysts. *Chem. Soc. Rev.* **44**, 5092-5147, doi:10.1039/c5cs00090d (2015).
- 3 Suib, S. L. *et al.* Some novel porous materials for selective catalytic oxidations. *Materials Today* **32**, 244-259, doi:10.1016/j.mattod.2019.06.008 (2020).
- 4 Croissant, J. G., Butler, K. S., Zink, J. I. & Brinker, C. J. Synthetic amorphous silica nanoparticles: toxicity, biomedical and environmental implications. *Nature Reviews Materials* **5**, 886-909, doi:10.1038/s41578-020-0230-0 (2020).
- 5 Kankala, R. K. *et al.* Nanoarchitected Structure and Surface Biofunctionality of Mesoporous Silica Nanoparticles. *Adv. Mater.* **32**, e1907035, doi:10.1002/adma.201907035 (2020).
- 6 Tang, F., Li, L. & Chen, D. Mesoporous silica nanoparticles: synthesis, biocompatibility and drug delivery. *Adv. Mater.* **24**, 1504-1534, doi:10.1002/adma.201104763 (2012).
- 7 Siegelman, R. L., Kim, E. J. & Long, J. R. Porous materials for carbon dioxide separations. *Nat. Mater.* **20**, 1060-1072, doi:10.1038/s41563-021-01054-8 (2021).
- 8 Cai, M. *et al.* Greenhouse-inspired supra-photothermal CO<sub>2</sub> catalysis. *Nature Energy* **6**, 807-814, doi:10.1038/s41560-021-00867-w (2021).
- 9 Wang, J. *et al.* Recent advances in solid sorbents for CO<sub>2</sub> capture and new development trends. *Energy & Environmental Science* **7**, 3478-3518, doi:10.1039/c4ee01647e (2014).
- 10 Zu, L. H. *et al.* Mesoporous Materials for Electrochemical Energy Storage and Conversion. *Advanced Energy Materials* **10**, doi:10.1002/aenm.202002152 (2020).
- 11 Yan, Y. X. *et al.* Mesoporous Nanoarchitectures for Electrochemical Energy Conversion and Storage. *Adv. Mater.* **32**, doi:10.1002/adma.202004654 (2020).
- 12 Li, W., Liu, J. & Zhao, D. Mesoporous materials for energy conversion and storage devices. *Nature Reviews Materials* **1**, doi:10.1038/natrevmats.2016.23 (2016).
- 13 Slater, A. G. & Cooper, A. I. Function-led design of new porous materials. *Science* **348**, doi:10.1126/science.aaa8075 (2015).
- 14 Gao, M., Zeng, J., Liang, K., Zhao, D. & Kong, B. Interfacial Assembly of Mesoporous Silica-Based Optical Heterostructures for Sensing Applications. *Adv. Funct. Mater.* **30**, doi:10.1002/adfm.201906950 (2020).
- 15 Boissiere, C., Grosso, D., Chaumonnot, A., Nicole, L. & Sanchez, C.

- Aerosol route to functional nanostructured inorganic and hybrid porous materials. *Adv. Mater.* **23**, 599-623, doi:10.1002/adma.201001410 (2011).
- 16 Malekzadeh, M. & Swihart, M. T. Vapor-phase production of nanomaterials. *Chem. Soc. Rev.*, doi:10.1039/d0cs01212b (2021).
- 17 Debecker, D. P., Le Bras, S., Boissiere, C., Chaumonnot, A. & Sanchez, C. Aerosol processing: a wind of innovation in the field of advanced heterogeneous catalysts. *Chem. Soc. Rev.* **47**, 4112-4155, doi:10.1039/c7cs00697g (2018).
- 18 Koirala, R., Pratsinis, S. E. & Baiker, A. Synthesis of catalytic materials in flames: opportunities and challenges. *Chem. Soc. Rev.* **45**, 3053-3068, doi:10.1039/c5cs00011d (2016).
- 19 Liu, S., Mohammadi, M. M. & Swihart, M. T. Fundamentals and recent applications of catalyst synthesis using flame aerosol technology. *Chem. Eng. J.* **405**, doi:10.1016/j.cej.2020.126958 (2021).
- 20 Teoh, W. Y., Amal, R. & Madler, L. Flame spray pyrolysis: An enabling technology for nanoparticles design and fabrication. *Nanoscale* **2**, 1324-1347, doi:10.1039/c0nr00017e (2010).
- 21 Schimmoeller, B., Pratsinis, S. E. & Baiker, A. Flame Aerosol Synthesis of Metal Oxide Catalysts with Unprecedented Structural and Catalytic Properties. *Chemcatchem* **3**, 1234-1256, doi:10.1002/cctc.201000425 (2011).
- 22 Lovell, E. C. *et al.* Asymmetrical Double Flame Spray Pyrolysis-Designed SiO<sub>2</sub>/Ce<sub>0.7</sub>Zr<sub>0.3</sub>O<sub>2</sub> for the Dry Reforming of Methane. *ACS Appl. Mater. Interfaces* **11**, 25766-25777, doi:10.1021/acsami.9b02572 (2019).
- 23 Paulson, N. H., Libera, J. A. & Stan, M. Flame spray pyrolysis optimization via statistics and machine learning. *Materials & Design* **196**, doi:10.1016/j.matdes.2020.108972 (2020).
- 24 Madler, L., Kammler, H. K., Mueller, R. & Pratsinis, S. E. Controlled synthesis of nanostructured particles by flame spray pyrolysis. *J. Aerosol Sci.* **33**, 369-389, doi:10.1016/s0021-8502(01)00159-8 (2002).
- 25 Schulz, H., Madler, L., Pratsinis, S. E., Burtscher, P. & Moszner, N. Transparent nanocomposites of radiopaque, flame-made Ta<sub>2</sub>O<sub>5</sub>/SiO<sub>2</sub> particles in an acrylic matrix. *Adv. Funct. Mater.* **15**, 830-837, doi:10.1002/adfm.200400234 (2005).
- 26 Scharmach, W. J., Buchner, R. D., Papavassiliou, V., Pacouloute, P. & Swihart, M. T. A High-Temperature Reducing Jet Reactor for Flame-Based Metal Nanoparticle Production. *Aerosol Sci. Technol.* **44**, 1083-1088, doi:10.1080/02786826.2010.511320 (2010).
- 27 Mohammadi, M. M. *et al.* Flame-synthesized nickel-silver nanoparticle inks provide high conductivity without sintering. *Chem. Eng. J.* **372**, 648-655, doi:10.1016/j.cej.2019.04.141 (2019).

- 28 Sharma, M. K. *et al.* Flame-driven Aerosol Synthesis of Copper-Nickel Nanopowders and Conductive Nanoparticle Films. *ACS Appl. Mater. Interfaces* **6**, 13542-13551, doi:10.1021/am5026853 (2014).
- 29 Debecker, D. P. *et al.* One-pot aerosol route to MoO<sub>3</sub>-SiO<sub>2</sub>-Al<sub>2</sub>O<sub>3</sub> catalysts with ordered super microporosity and high olefin metathesis activity. *Angew. Chem. Int. Ed. Engl.* **51**, 2129-2131, doi:10.1002/anie.201106277 (2012).
- 30 Zhang, F., Kang, C., Wei, Y. & Li, H. Aerosol-Spraying Synthesis of Periodic Mesoporous Organometalsilica Spheres with Chamber Cavities as Active and Reusable Catalysts in Aqueous Organic Reactions. *Adv. Funct. Mater.* **21**, 3189-3197 (2011).
- 31 Bore, M. T., Marzke, R. F., Ward, T. L. & Datye, A. K. Aerosol synthesized mesoporous silica containing high loading of alumina and zirconia. *J. Mater. Chem.* **15**, doi:10.1039/b503103f (2005).
- 32 Colbeau-Justin, F., Boissière, C., Chaumonnot, A., Bonduelle, A. & Sanchez, C. Aerosol Route to Highly Efficient (Co)Mo/SiO<sub>2</sub> Mesoporous Catalysts. *Adv. Funct. Mater.* **24**, 233-239, doi:10.1002/adfm.201302156 (2014).
- 33 Kho, K. & Hadinoto, K. Aqueous re-dispersibility characterization of spray-dried hollow spherical silica nano-aggregates. *Powder Technol.* **198**, 354-363, doi:10.1016/j.powtec.2009.11.031 (2010).
- 34 Wu, Z. X. *et al.* Spray-drying water-based assembly of hierarchical and ordered mesoporous silica microparticles with enhanced pore accessibility for efficient bio-adsorption. *J. Colloid Interface Sci.* **556**, 529-540, doi:10.1016/j.jcis.2019.08.084 (2019).
- 35 Yilmaz, M. S. Synthesis of novel amine modified hollow mesoporous silica@Mg-Al layered double hydroxide composite and its application in CO<sub>2</sub> adsorption. *Microporous Mesoporous Mater.* **245**, 109-117, doi:10.1016/j.micromeso.2017.02.077 (2017).
- 36 Liu, S., Chen, X., Ai, W. & Wei, C. A new method to prepare mesoporous silica from coal gasification fine slag and its application in methylene blue adsorption. *Journal of Cleaner Production* **212**, 1062-1071, doi:10.1016/j.jclepro.2018.12.060 (2019).
- 37 Zhuravlev, L. T. The surface chemistry of amorphous silica. Zhuravlev model. *Colloids and Surfaces a-Physicochemical and Engineering Aspects* **173**, 1-38, doi:10.1016/s0927-7757(00)00556-2 (2000).
- 38 Li, K. *et al.* A Generic Method for Preparing Hollow Mesoporous Silica Catalytic Nanoreactors with Metal Oxide Nanoparticles inside Their Cavities. *Angew. Chem. Int. Ed. Engl.* **57**, 16458-16463, doi:10.1002/anie.201810777 (2018).
- 39 Wang, H. *et al.* Facile fabrication of noble metal nanoparticles encapsulated in hollow silica with radially oriented mesopores: multiple roles of the N-lauroylsarcosine sodium surfactant. *Chem.*

- Commun. (Camb.)* **47**, 7680-7682, doi:10.1039/c1cc12823j (2011).
- 40 Rafatullah, M., Sulaiman, O., Hashim, R. & Ahmad, A. Adsorption of methylene blue on low-cost adsorbents: A review. *J. Hazard. Mater.* **177**, 70-80, doi:10.1016/j.jhazmat.2009.12.047 (2010).
- 41 Moghaddam, S. P. H., Yazdimamaghani, M. & Ghandehari, H. Glutathione-sensitive hollow mesoporous silica nanoparticles for controlled drug delivery. *J. Control. Release* **282**, 62-75, doi:10.1016/j.jconrel.2018.04.032 (2018).
- 42 Xu, X. *et al.* Naturally Dried Graphene Aerogels with Superelasticity and Tunable Poisson's Ratio. *Adv. Mater.* **28**, 9223-+, doi:10.1002/adma.201603079 (2016).
- 43 An, L. *et al.* An All-Ceramic, Anisotropic, and Flexible Aerogel Insulation Material. *Nano Lett.* **20**, 3828-3835, doi:10.1021/acs.nanolett.0c00917 (2020).
- 44 Liu, S. *et al.* Flame aerosol synthesis of hollow alumina nanoshells for application in thermal insulation. *Chem. Eng. J.* **428**, doi:10.1016/j.cej.2021.131273 (2022).
- 45 Li, Y. & Shi, J. Hollow-structured mesoporous materials: chemical synthesis, functionalization and applications. *Adv. Mater.* **26**, 3176-3205, doi:10.1002/adma.201305319 (2014).
- 46 Hampsey, J. E., Arsenault, S., Hu, Q. Y. & Lu, Y. F. One-step synthesis of mesoporous metal-SiO<sub>2</sub> particles by an aerosol-assisted self-assembly process. *Chem. Mater.* **17**, 2475-2480, doi:10.1021/cm0487167 (2005).
- 47 Fukuoka, A., Kimura, J. I., Oshio, T., Sakamoto, Y. & Ichikawa, M. Preferential oxidation of carbon monoxide catalyzed by platinum nanoparticles in mesoporous silica. *J. Am. Chem. Soc.* **129**, 10120-10125, doi:10.1021/ja0703123 (2007).
- 48 Satter, S. S., Hirayama, J., Kobayashi, H., Nakajima, K. & Fukuoka, A. Water-Resistant Pt Sites in Hydrophobic Mesopores Effective for Low-Temperature Ethylene Oxidation. *Acs Catalysis* **10**, 13257-13268, doi:10.1021/acscatal.0c02816 (2020).
- 49 Zhu, J. J., Wang, T., Xu, X. L., Xiao, P. & Li, J. L. Pt nanoparticles supported on SBA-15: Synthesis, characterization and applications in heterogeneous catalysis. *Applied Catalysis B-Environmental* **130**, 197-217, doi:10.1016/j.apcatb.2012.11.005 (2013).
- 50 Lim, Z.-Y., Tu, J., Xu, Y. & Chen, B. Enhanced porosity of Ni@Hollow meso-SiO<sub>2</sub> catalyst for CO<sub>2</sub> reforming of methane. *Int. J. Hydrogen Energy* **46**, 7866-7877, doi:10.1016/j.ijhydene.2020.09.204 (2021).
- 51 Wang, K. *et al.* Decoupling the size and support/metal loadings effect of Ni/SiO<sub>2</sub> catalysts for CO<sub>2</sub> methanation. *Fuel* **304**, doi:10.1016/j.fuel.2021.121388 (2021).
- 52 Atsumi, R. *et al.* Ammonia decomposition activity over Ni/SiO<sub>2</sub> catalysts with different pore diameters. *Int. J. Hydrogen Energy* **39**,

- 13954-13961, doi:10.1016/j.ijhydene.2014.07.003 (2014).
- 53 He, Y. *et al.* Research on the Selectivity and Activity of Ethane Oxidation Dehydrogenation with CO<sub>2</sub> on Cr-based Catalyst. *Chemistryselect* **5**, 2232-2239, doi:10.1002/slct.201904842 (2020).
- 54 Atanga, M. A., Rezaei, F., Jawad, A., Fitch, M. & Rownaghi, A. A. Oxidative dehydrogenation of propane to propylene with carbon dioxide. *Applied Catalysis B: Environmental* **220**, 429-445, doi:10.1016/j.apcatb.2017.08.052 (2018).
- 55 Martino, G. A. *et al.* Rationalizing the Effect of Triethylaluminum on the Cr/SiO<sub>2</sub> Phillips Catalysts. *Acs Catalysis* **10**, 2694-2706, doi:10.1021/acscatal.9b04726 (2020).
- 56 Yao, Y. G. *et al.* Carbothermal shock synthesis of high-entropy-alloy nanoparticles. *Science* **359**, 1489-1494, doi:10.1126/science.aan5412 (2018).
- 57 Li, T. *et al.* Denary oxide nanoparticles as highly stable catalysts for methane combustion. *Nature Catalysis* **4**, 62-70, doi:10.1038/s41929-020-00554-1 (2021).
- 58 Kwon, O. *et al.* Exsolution trends and co-segregation aspects of self-grown catalyst nanoparticles in perovskites. *Nat. Commun.* **8**, 15967, doi:10.1038/ncomms15967 (2017).
- 59 Joo, S. *et al.* Highly active dry methane reforming catalysts with boosted in situ grown Ni-Fe nanoparticles on perovskite via atomic layer deposition. *Science Advances* **6**, doi:10.1126/sciadv.abb1573 (2020).
- 60 Joo, S. *et al.* Enhancing Thermocatalytic Activities via Up-shift of the d-Band Center of Exsolved Co-Ni-Fe Ternary Alloy Nanoparticles for Dry Reforming of Methane. *Angew. Chem. Int. Ed. Engl.*, doi:10.1002/anie.202101335 (2021).
- 61 Song, Y. *et al.* Dry reforming of methane by stable Ni-Mo nanocatalysts on single-crystalline MgO. *Science* **367**, 777-781 (2020).
- 62 Guo, S. P. *et al.* A comprehensive insight into the role of barium in catalytic performance of Co/Al<sub>2</sub>O<sub>3</sub> catalyst for Fischer-Tropsch synthesis. *Fuel* **256**, doi:10.1016/j.fuel.2019.115911 (2019).
- 63 Li, X., Wang, P., Wang, H. & Li, C. Effects of the state of Co species in Co/Al<sub>2</sub>O<sub>3</sub> catalysts on the catalytic performance of propane dehydrogenation. *Appl. Surf. Sci.* **441**, 688-693, doi:10.1016/j.apsusc.2018.02.024 (2018).
- 64 Horlyck, J. *et al.* Unifying double flame spray pyrolysis with lanthanum doping to restrict cobalt-aluminate formation in Co/Al<sub>2</sub>O<sub>3</sub> catalysts for the dry reforming of methane. *Catalysis Science & Technology* **9**, 4970-4980, doi:10.1039/c9cy01293a (2019).
- 65 Pakhare, D. & Spivey, J. A review of dry (CO<sub>2</sub>) reforming of methane

over noble metal catalysts. *Chem. Soc. Rev.* **43**, 7813-7837,  
doi:10.1039/c3cs60395d (2014).